

Design and Performance Characterization of an Additively Manufactured Primary Heat Exchanger for sCO₂ Waste Heat Recovery Cycles

E. Rasouli
Post-doctoral Scholar
Mechanical and Aerospace Engineering
University of California, Davis
Davis, CA

S. Subedi
Graduate Student
Material Science and Engineering
Carnegie Mellon University
Pittsburgh, PA

C. Montgomery
Graduate Student
Mechanical Engineering
Carnegie Mellon University
Pittsburgh, PA

C. W. Mande
Associate Engineer
Western Cooling Efficiency Center
University of California, Davis
Davis, CA

M. Stevens
Assistant Engineer
Western Cooling Efficiency Center
University of California, Davis
Davis, CA

V. Narayanan
Professor
Mechanical and Aerospace Engineering
University of California, Davis
Davis, CA

A. D. Rollett
Professor
Material Science and Engineering
Carnegie Mellon University
Pittsburgh, PA

ABSTRACT

Design, fabrication and characterization of an additively manufactured (AM) Inconel 718 Primary Heat Exchanger (PHX) for waste heat recovery is discussed. Design details including considerations of pressure drop on the hot side, high internal pressure on the sCO₂ side and the near-counter flow design for high effectiveness are discussed. The fabricated AM PHX is pressure tested at temperature for verification of structural integrity. Preliminary results of pressure drop and heat transfer rate are also presented.

INTRODUCTION

The supercritical carbon dioxide (sCO₂) Brayton cycle has gained attention in recent years due to the potential for high cycle efficiency at moderate turbine inlet temperatures between 450-700 °C. Several researchers are investigating use of this power cycle with varied sources such as fossil, solar, nuclear, geothermal, and moderate- to high-quality waste heat streams [1]. For waste heat recovery power cycles, it is necessary to design an efficient heat exchanger that can be placed in the waste heat stream, such as the exhaust of a gas turbine, and transfer heat into the sCO₂ stream. This heat exchanger would be the Primary Heat Exchanger (PHX) for the sCO₂ cycle since it is at the high temperature end of the cycle. Key considerations in the design of such a PHX include high effectiveness, the ability to withstand high internal pressures, large pressure difference between the two fluid streams, low pressure drop across the waste heat stream and reliability under thermal cycling. Traditional heat recuperators consist of finned tube heat

exchangers with flue gas going through the finned section and liquid flowing through the tubes. Fins are located on the flue gas side to increase the surface area for heat transfer on the side with the largest thermal resistance. While finned tube heat exchangers lend to compact designs with higher overall heat transfer coefficients, they are limited by heat conduction through the fins. Fin efficiency considerations could necessitate use of larger number of tube passes, thereby increasing the pressure drop through the recuperator. Furthermore, traditional finned tube heat exchangers are also arranged in cross-flow configuration to the flue gas, thereby placing a limit on the effectiveness of heat exchange.

In this paper, the design, fabrication and preliminary thermal-fluidic characterization of an additively manufactured (AM) PHX with microscale features is discussed. The PHX design, discussed in the next section, allows for a near-counter flow between the $s\text{CO}_2$ and flue gas streams. In contrast with a finned tube design, a plate-type design is used wherein each of the fins in the traditional finned tube heat exchanger becomes a “cold plate” through which $s\text{CO}_2$ flows directly. The $s\text{CO}_2$ stream flows through an array of microscale pin fins within each plate. A pin fin architecture is used for the microscale regions since it lends to higher heat transfer rate and better flow distribution than parallel microchannels [2,3].

Inconel 718, a nickel-chromium based superalloy with 50-55% nickel, 17-21% chromium, 4.57-5.5% niobium, 2.80-3.30% molybdenum and trace amount of other compounds, is used for fabrication of the PHX. It is a high-strength (tensile strength exceeding 1.4 GPa), corrosion and oxidation resistant, superalloy that can operate at temperatures of -423 °F to 1300 °F. The term “superalloys” refers to a high performance alloy that exhibits properties such as excellent mechanical strength, resistance to creep deformation and rupture, good surface stability, and resistance to corrosion [4,5]. The specific AM technique used in this work is direct metal laser sintering (DMLS). Although the name DMLS suggests sintering, which means that the powder particles are compacted below its liquefaction point, there is no sintering of powder in the utilized AM system (EOS M290). The design and fabrication details of the PHX are first provided, followed by a preliminary characterization of pressure drop and heat transfer.

PRIMARY HEAT EXCHANGER DESIGN

As is depicted in Figure 1a, the concept for PHX consists of several cold plates spaced a certain distance (S_{plate}) apart and connected to distributor and collector $s\text{CO}_2$ manifolds. These plates are placed in a stream of the hot combustion gases. The cold plates are micro-pin fin plates through which $s\text{CO}_2$ flows in a near-counter flow direction to the hot gases. To enhance the heat transfer coefficient on the hot side, fin structures are designed on the outer surface of the cold plates such that they connect one plate to its adjacent cold plates, see inset picture in Figure 1a- (fins are shown in black color).

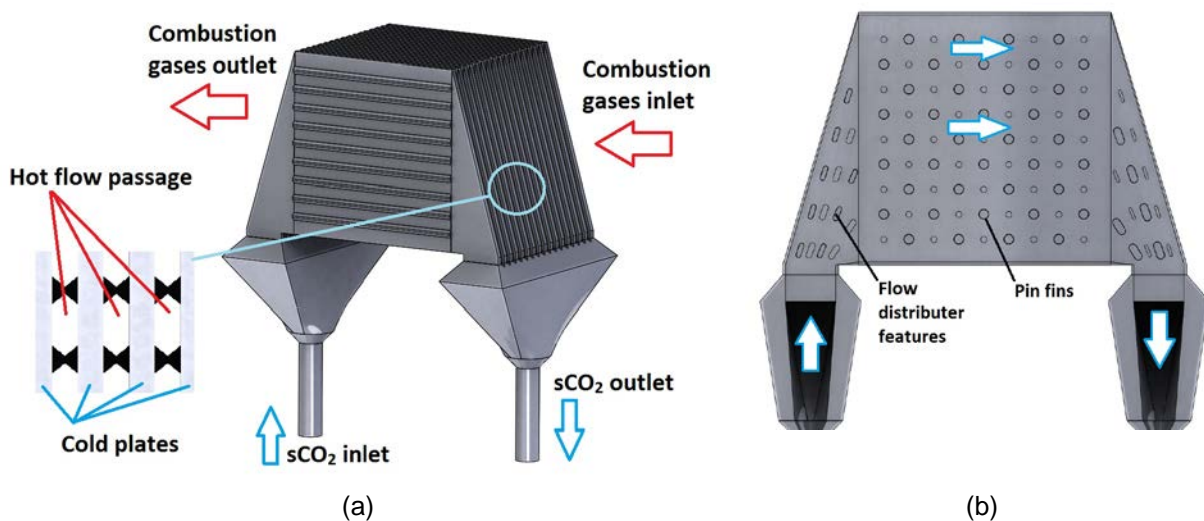


Figure 1. 3D model proposed for PHX a) overall view illustrating several cold plates with specified spacing connected to inlet and outlet plena. b) view of micro features within a cold plate.

Within each cold plate microchannel, as shown in Figure 1b, there are two types of micro structures which are mechanically holding the internal channel together against high system pressure (200 bar). Moreover the micro structures on the inlet and outlet triangular plenums of a cold plate have to be designed such that flow is distributed uniformly along the width of the plate. The design of micro pin fins along the length of the cold plate is critical in enhancing the heat transfer and determining subsequent sCO₂ pressure drop.

There are several important parameters in determining the overall size of this PHX design such as cross section dimensions of the duct carrying hot gases, cold plates spacing, fin spacing, cold plate pin fin geometry design, hot and cold flow inlet temperatures, heat load capacity, and PHX material. A parametric study was performed on a square duct with cross section size of 0.635 m x 0.635 m (24x24 in²) carrying hot gases. A PHX made out of Inconel 718 with effectiveness of 0.9 and sCO₂ inlet temperature ($T_{c,i}$) and pressure of 250°C and 200 bar, respectively, was considered. The fin spacing was kept identical to cold plate spacing. For simplicity, the cold plate internal design for this parametric study was assumed as a microgap with 500 μ m channel height without any micro pin fins within the microchannel plate. Micro-pin-fin array heat transfer correlations such as that by Rasouli et al. [6] can be used to more accurately quantify the thermal and hydrodynamic performance of each cold plate. The results are not expected to change significantly by use of pin array correlations on the cold side since the larger resistance to heat transfer in the PHX is on the hot side. The hot gases inlet temperature ($T_{h,i}$) was selected to be 800°C and sCO₂ outlet temperature ($T_{c,o}$) at 700°C. With the assumed effectiveness, the selected parameters resulted in a PHX heat load of ~2 MW.

Parametric studies on the variation of primary HX length and hot side pressure drop with plate spacing, S_{plate} , was then performed and the results are shown in Figure a. A design with smaller plate spacing would have larger number of the plates for the given duct size; hence, in order to attain to the required heat transfer surface area, the length of cold plate could be shorter. Reducing the plate spacing increases the pressure drop because the size of the hot flow passages decrease (see inset picture in Figure 1a). At the smallest analyzed spacing value (2.8 mm) and a HX length of 0.86 m, the pressure drop was less than 0.35 bar (~34.1 kPa), see Figure 2a.

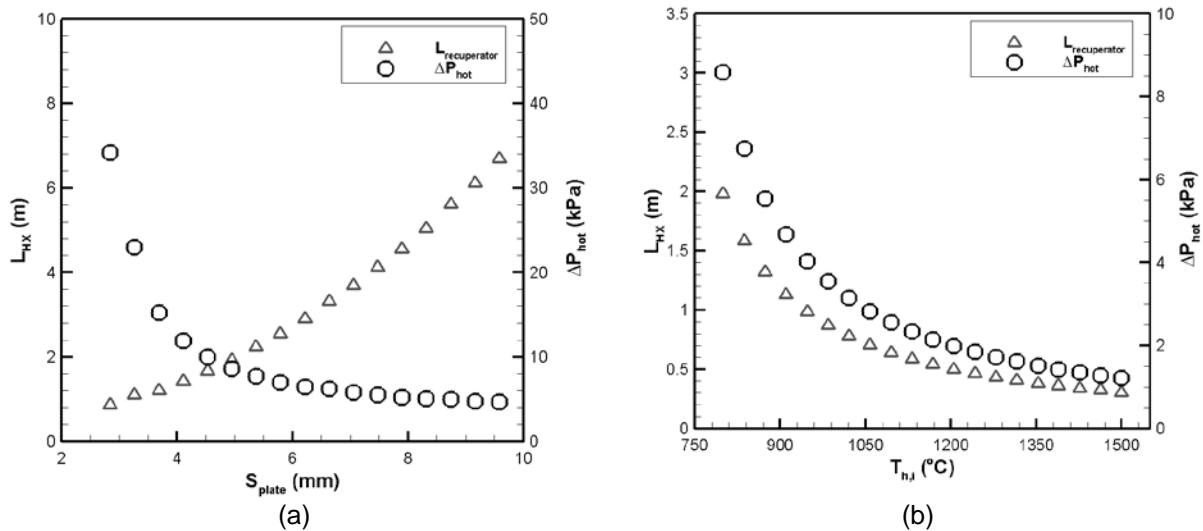


Figure 2. Variation of 2 MW PHX length and hot side pressure drop a) with cold plate spacing and b) with hot side inlet temperature, $T_{h,i}$.

Variation of PHX length and hot side pressure drop with $T_{h,i}$ is depicted in Figure 2b. Held constant were the HX heat load of 2 MW, fin and plate spacing at 5 mm, and $T_{c,o}$ at 700°C. The $T_{c,o}$ was kept constant at 700 °C by reducing the mass flow rate on the hot side with increasing $T_{h,i}$. It was seen that increasing the hot side inlet temperature significantly reduces the length of the primary HX and resulted in a lower pressure drop. This trend was primarily driven by the reduction in flow rate at higher inlet temperature for a fixed rating of the PHX.

These promising results of a compact PHX prompted development of a scaled PHX using AM fabrication to be fitting in a duct with cross section of 5 x 5 cm². Based on the design feedback from AM process, a minimum wall thickness for this design was set as 500 μm and the over-hanged features with respect to AM fabrication direction (those with 90° angle) were replaced by moderate angles (<45°).

Structural and CFD analysis was performed on the plates in order to have a viable design to withstand 200 bar internal pressure while having uniform flow distribution in its cold plates. First, mechanical integrity simulations using Ansys Mechanical APDL was performed; the results following several design iterations are shown in Figure 3. The absolute pressure of 200 bar was imposed on all the internal surfaces of a cooling plate while the outer exposed surfaces were left at atmosphere pressure (1 bar). Due to symmetry of the plate only half of the plate was meshed. The tensile yield strength of Inconel 718 at 538 °C (1000 °F) is 1020 MPa. The mechanical simulations showed that the equivalent stress almost everywhere within the cooling plate were below 700 MPa. There are no cells in the side plenums with stresses higher than 500 MPa.

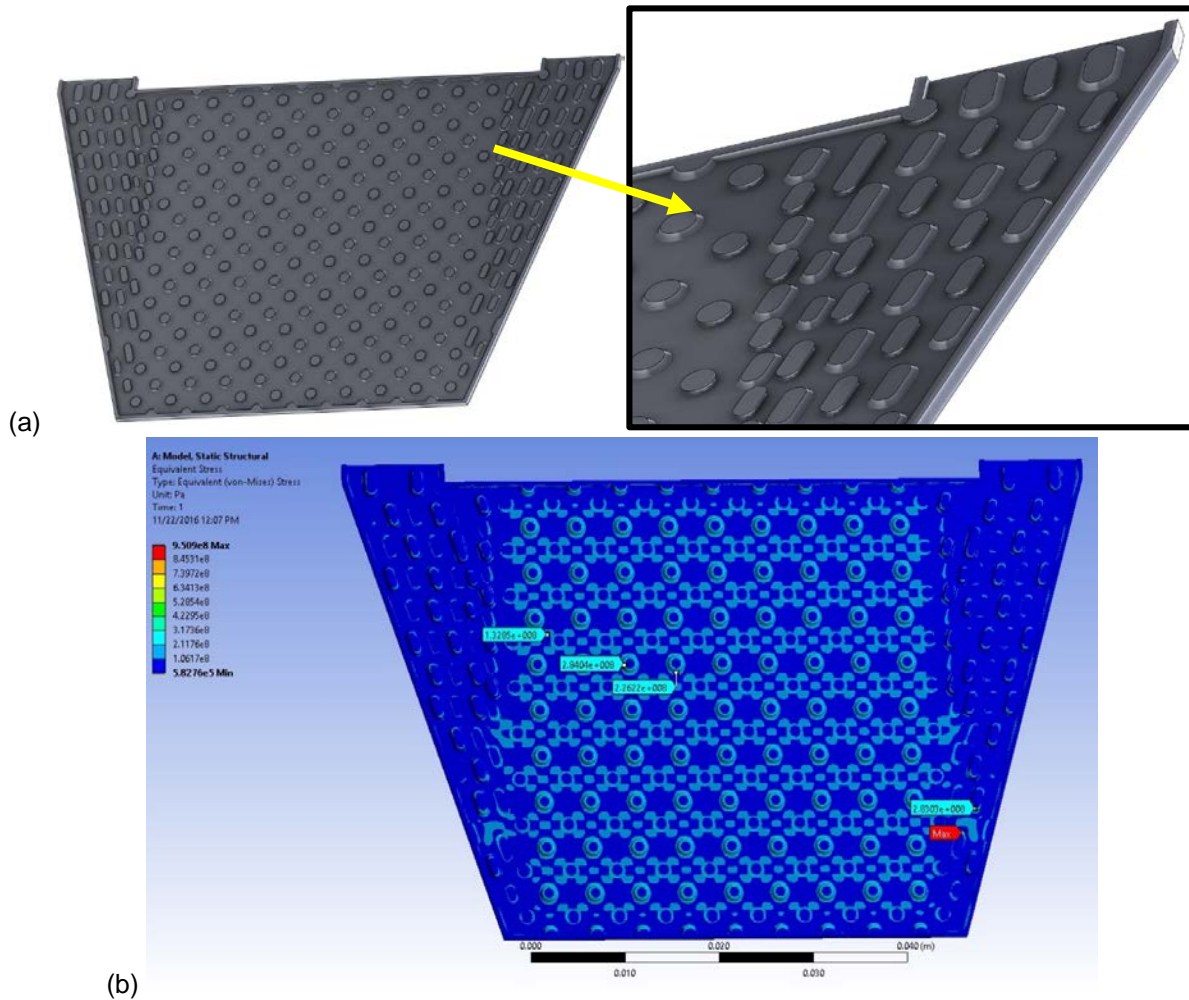


Figure 3. Final design and mechanical simulation on the refined cooling plate of the primary HX. (a) Final design of a cooling plate- overall plate left, zoom in on the plenum section right, (b) Equivalent Von-Mises stress contours- safety factor greater than unity everywhere within the plate

Upon verification of the structural aspects of the design, computational fluid dynamics (CFD) simulations were performed to ensure uniform flow distribution across the cooling plate. The velocity magnitude contours in the mid-plane between top and bottom walls are shown in Figure 4a. The design inlet mass

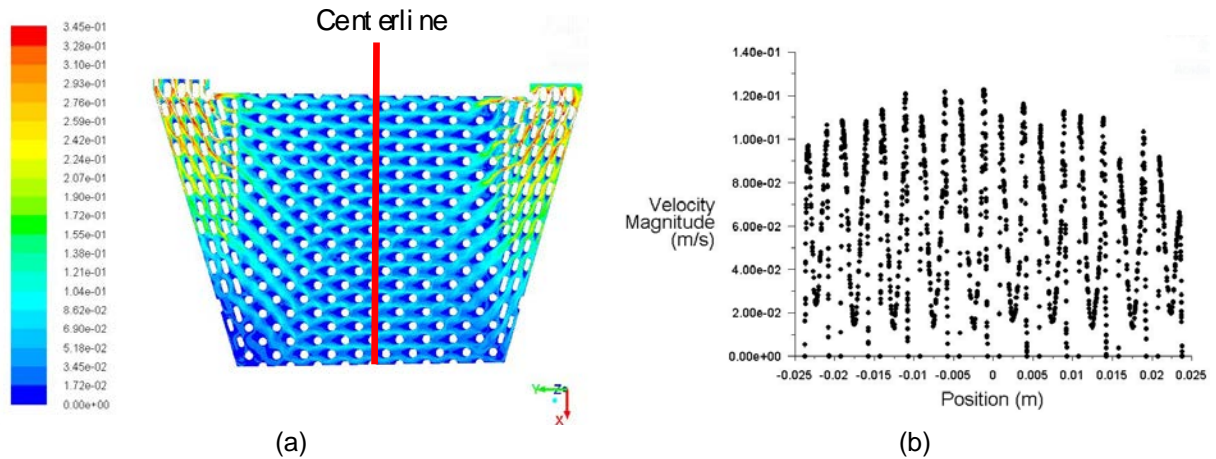


Figure 4. a) Velocity magnitude contours in the mid-plane b) Velocity magnitude along the centerline.

flowrate to each cooling plate is ~ 0.11 g/s which corresponds to 0.103 m/s inlet velocity which was used as the boundary condition at the inlet. The pressure outlet boundary condition was used at the outlet of the plate while no-slip boundary condition was imposed to all other surfaces. The velocity magnitude along the centerline (marked in Figure 4a) is shown in Figure 4b which confirms acceptable flow uniformity.

Mechanical design simulations were also performed on the inlet and exit plenums which connect all cooling plates together; details of header design are not discussed here for brevity. In order to increase heat transfer on the hot side of HX, the external fin shapes were altered in two other design variations- the first involved use of curved fins (see Figure 5a) and offset strip fins (see Figure 5b). The fin shape design iterations were performed for a sub-scale PHX which had only 3 cooling plates to reduce AM fabrication time and cost. The idea behind the offset fins was to increase the developing flow region and enhance the hot side heat transfer. In addition to the increased surface area on the hot side, the curved fin design also served to increase the length of counter flow based on the velocity stream lines of the cold stream (sCO_2) inside the cooling plates- compare Figure 5a with Figure 4a. The design of ~ 500 W PHX had 17 cooling plates and the sub-scale PHXs had 3 plates.

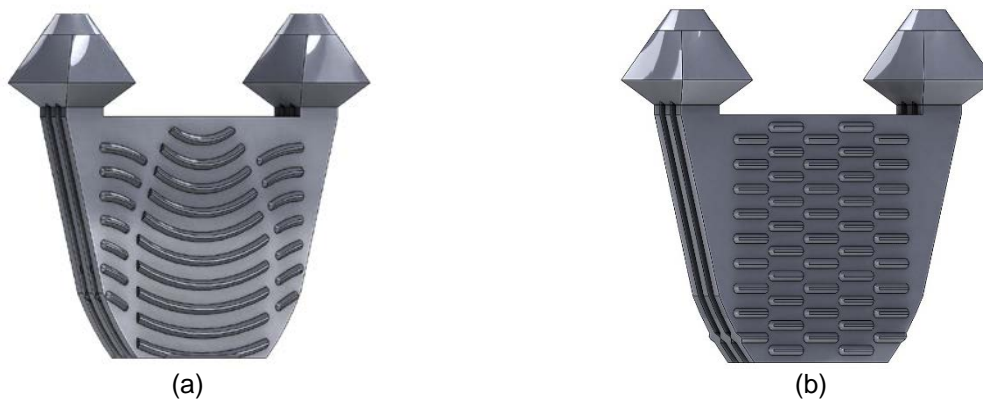


Figure 5. Variants of the 3-plate PHX designs to enhance hot side heat transfer coefficient a) stripped fins b) curvy fins

PHX FABRICATION

The Carnegie Mellon University EOS M290 AM machine is shown in Figure a, and the build plate and laser melting is shown in Figure 6b. The recoater arm from the right spreads the powder to the left side of the compartment on the build platform. Up to 400 W fiber laser beam was used for high quality and precision. The build platform moves down, and the powder dispenser platform moves up after every successful layer spread and melting. The excess powder is collected in the hopper. The build platform is generally heated to a low temperature i.e. 95 – 392 °C. The subsequent spreading and melting of powder is done until the part is fully built.

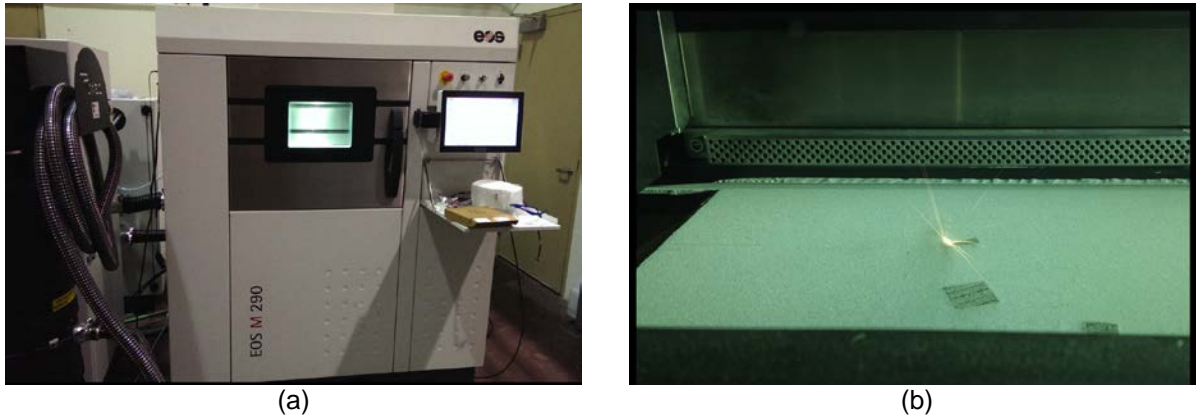


Figure 6 a) EOS AM machine at CMU b) build plate showing laser melting of powder.

The steps of creating a computer aided design (CAD) to printing is shown in Figure 7. First a CAD design was created (step 1), using SolidWorks™ in this case, converted to .stl and uploaded to a software called Magics™ (step 2). Magics™ adds support to the part as shown by the structure in yellow. It also checks the contiguity of the part and provides feedback if there are any dissembled or misaligned joints. After Magics™, the file is transported to EOS print software (step 3) where the part is sliced according to the defined layer thickness. Next, process conditions such as power and velocity of the laser beam, pre and post contour beam settings, layer thickness, exposure and other parameters are also defined. The resulting file is then uploaded to the EOS machine (step 4) and the parts are printed to get the final product as shown in Figure 7 in step 5.

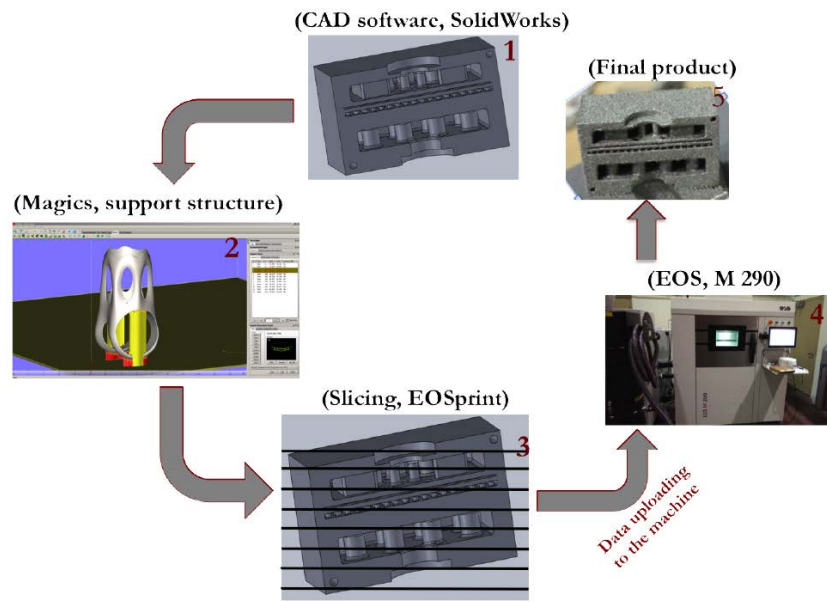
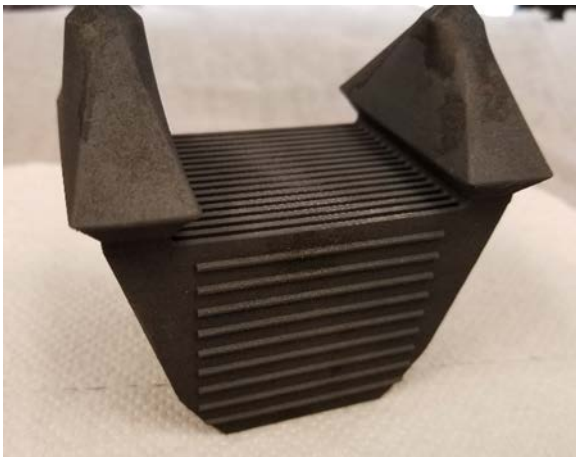


Figure 7. Schematics of various stages of metal printing, from design to fabrication.

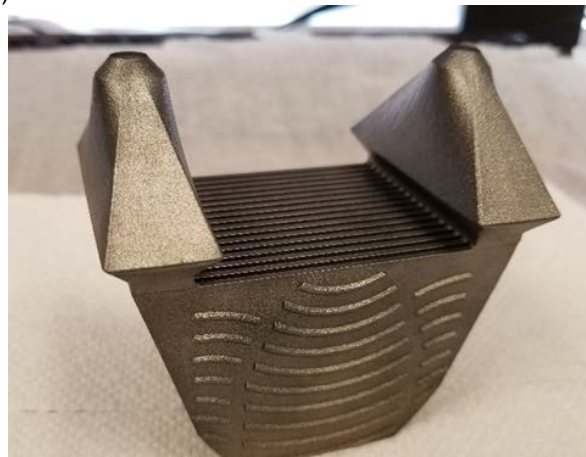
Gas atomized powder provided and/or approved by EOS was used in the fabrication process. The average powder particle size for Inconel 718 was 40 μm . The powder used in EOS is much finer than in an electron beam systems and hence provides a higher resolution and a better surface finish than an electron beam. An image of the build plate from the final build is shown in Figure a. It is clear that all 3-plate and 17-plate PHXs were successfully fabricated. The PHXs were subsequently heat treated (see Figure for example). Additionally, some of the PHX were sand blasted to improve surface finish (see Figure 8c).



(a)



(b)



(c)

Figure 8. Pictures of the final round of AM primary heat exchanger. (a) build plate upon completion of the AM fabrication, (b) heat treated 17-plate HX, (c) heat treated and sand blasted 17-plate HX

Fluid was used to flush the PHXs both internally and externally to remove excess powder. It was later determined that there was still significant powder lodged in between the fins and plates and additional cleaning was needed. The PHXs were immersed in an ultrasonic bath and acetone bath in an attempt to remove additional powder. While a significant number of passages could be cleared up using this approach, some passages were still clogged. A single 17-plate cleaned PHX was tested for integrity and characterized for heat transfer and pressure drop.

EXPERIMENTAL FACILITY

Pressure & Temperature test facility

The pressure and temperature (P&T) test facility was used to test the mechanical integrity of the AM PHX through static pressure testing at temperature. The facility consisted of a 500,000 BTU/hr natural gas burner connected to a steel P&T test chamber by a 21-inch diameter quick connect rigid steel ducting. Both the ducting and chamber were lined with high-temperature cellulose insulation. Compressed nitrogen gas was used for pressurizing the test articles. The assembled P&T facility is shown in Figure 9a. The 17-plate PHX was placed on top of refractory firebricks within the chamber as shown in Figure 9b and c. An electronically controlled pressure regulator and 3-way valve were used to control the pressure inside the PHX (seen in Figure 9a). The regulator was capable of adjusting the pressure of the line between 1- 200 bar based on the set pressure in a LabVIEW program. The electronically-controlled 3-way valve, located on the upstream of the pressure regulator, was also controlled by the same program and was used to isolate the PHX from the nitrogen tank during testing and purge the accumulated pressure in the line at the end of each cycle. The temperature was measured using k-type thermocouples that were placed in-between the plates of the PHX- see Figure 9c. The temperature and line pressure data were recorded in LabVIEW at a rate of 4Hz.

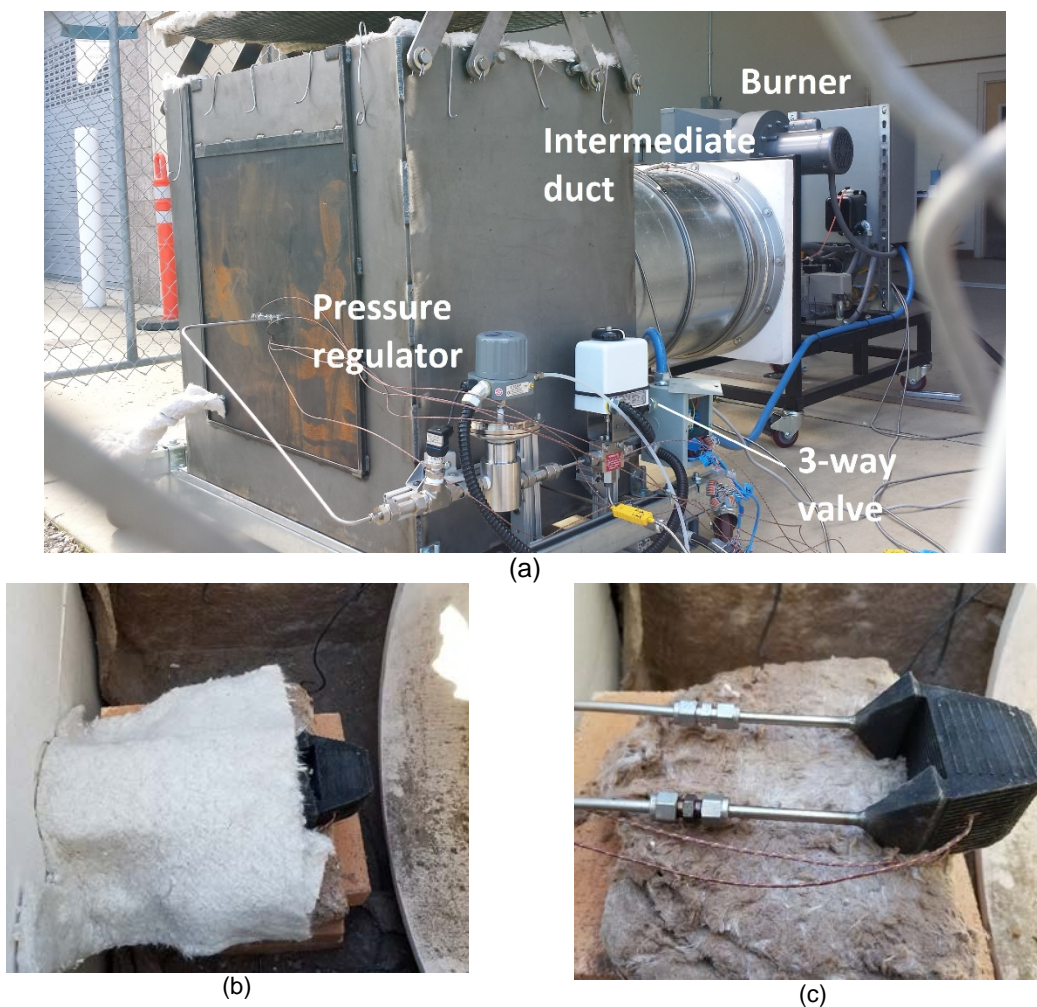


Figure 9. Pictures of the P&T facility. (a) overview of facility showing the chamber, duct and burner, (b) 17-plate PHX with insulation located within the chamber, and (c) detail of the PHX showing the location of the thermocouples.

Thermal-fluidic test facility

A sCO₂ flow loop used for heat transfer testing PHX is shown schematically in Figure 10 and consists of five major sub-systems; 1) a gas charging section, 2) a pump and reservoir section, 3) a flow pre-heating

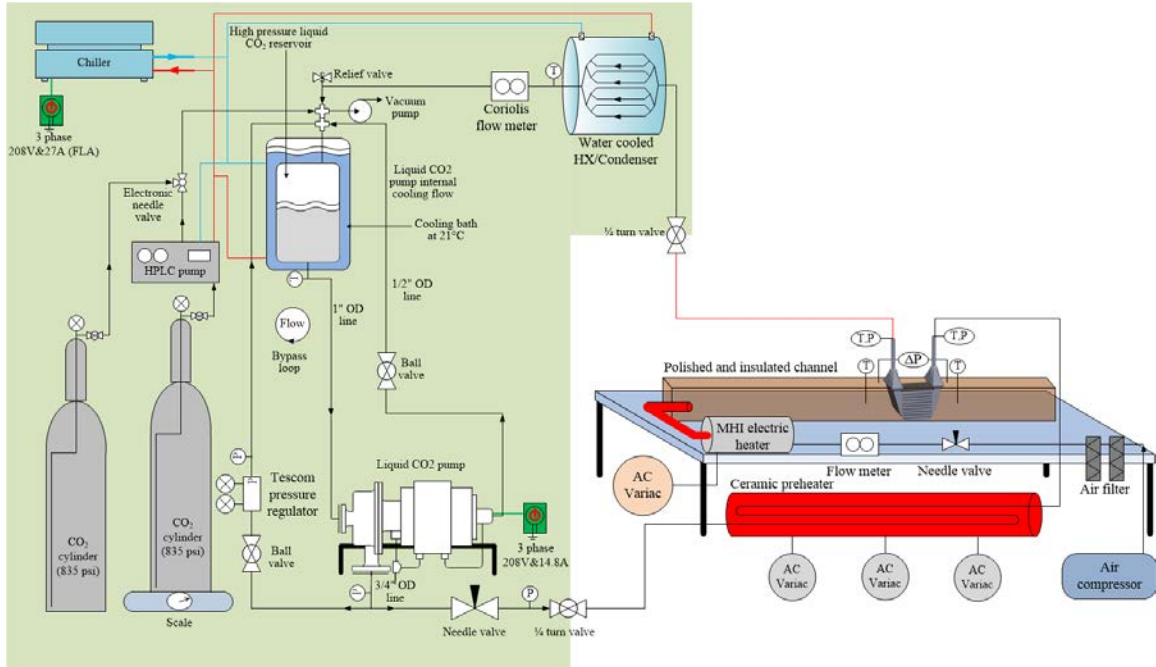


Figure 10. Schematic of the thermal-fluidic test facility

section, 4) a heat rejection and condenser section, and 5) a heated air channel open-loop. A combination of stainless steel 316 tube with 0.75in and 0.25in OD tubes with proper wall thickness was used for flow lines in this test facility. The tube material and sizing were selected based on required strength against 200 bar internal pressure (at temperatures up to 550 °C) and lowest possible line pressure drop.

The gas charging section consisted of several cylinders of CO₂. A HPLC pump located in the pump and reservoir section was connected to the cylinders and used to raise the system pressure close to the target pressure of ~200 bar. Prior to charging, a vacuum pump was used to evacuate the line in order to reduce the effect of contaminants and non-condensables. An electronically controlled three-way valve was located between the HPLC pump and the reservoir to permit charging the lines, closed loop operation, or release of CO₂ from the lines at the end of the experiment.

CO₂ was circulated through the loop using a two-stage high-pressure regenerative turbine pump (Teikoku chempump). This pump used the working fluid to provide cooling for the turbomachinery and hence requires a reverse circulation plumbing set up for sCO₂. A high pressure accumulator served as the reservoir for the fluid. The preheating section consisted of a custom made tubular ceramic heater (3 ft long) with three segregated heating elements each wired to a 120 V AC variac. Three passes of SS316 0.25in OD tube were inserted into the preheater where liquid CO₂ with above critical pressure became supercritical CO₂ (> 50 °C) by passing through the tube even at the highest tested flow rates (> 5g/s). The outlet flow from the PHX was cooled to below ~10 °C before returning to the liquid CO₂ pump using a 5-ton air-cooled chiller.

The PHX was placed inside a 5 cm x 5 cm stainless-steel channel that was insulated on the outside. Air was supplied using a compressor. The air was filtered, regulated, and metered to provide the desired flow rate of the hot side. An annotated image of the heated channel open-air loop is shown in Figure 11. An electric heater was used to heat the air prior to flowing through the channel. A 208 V AC variac was used to power the heater which depending on the set voltage and air flow rate, temperature up to 400 °C could be attained at the inlet of PHX hot side. Temperatures were recorded at the inlet and exit of the air stream as well as the CO₂ streams. The pressure drop on the heated air side was measured using a high-accuracy pressure transducer (uncertainty of ±0.02% FS, or 7 Pa). The air flow at the exit of the PHX was exhausted to the ambient.

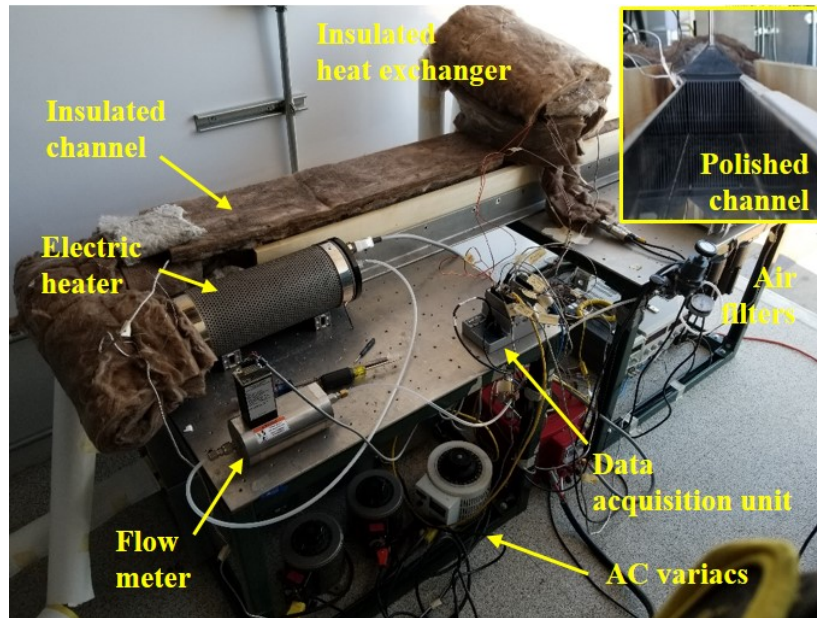


Figure 11. Annotated image of the heated channel open-air loop

RESULTS AND DISCUSSION

Figure 12 shows the results of static pressure tests for one of the 17-plate PHX with straight fins on the hot side (see Figure 9c). The PHX was installed in the P&T facility shown in Figure 9. One side was capped while the other end was connected to the high pressure nitrogen source. The first test was performed at ambient temperature; results are shown in Figure 12a. As seen from the Figure 12a, the PHX was able to withstand an internal pressure of ~200 bar. Next, the pressure was released and the burner was turned on to bring the external temperature of the PHX to ~550 °C, which is the design operating condition. The static pressure test was once again performed at this elevated temperature. Results from the high temperature test, shown in Figure 12b, indicate that the PHX was structurally sound at operating temperatures and pressure. The slight change in pressure at 200 bar between 60 and 80 minutes was caused by a leak in the fitting connecting the PHX to the regulator. This leak was rectified around the 80 minutes timeframe beyond which the pressure remained stable.

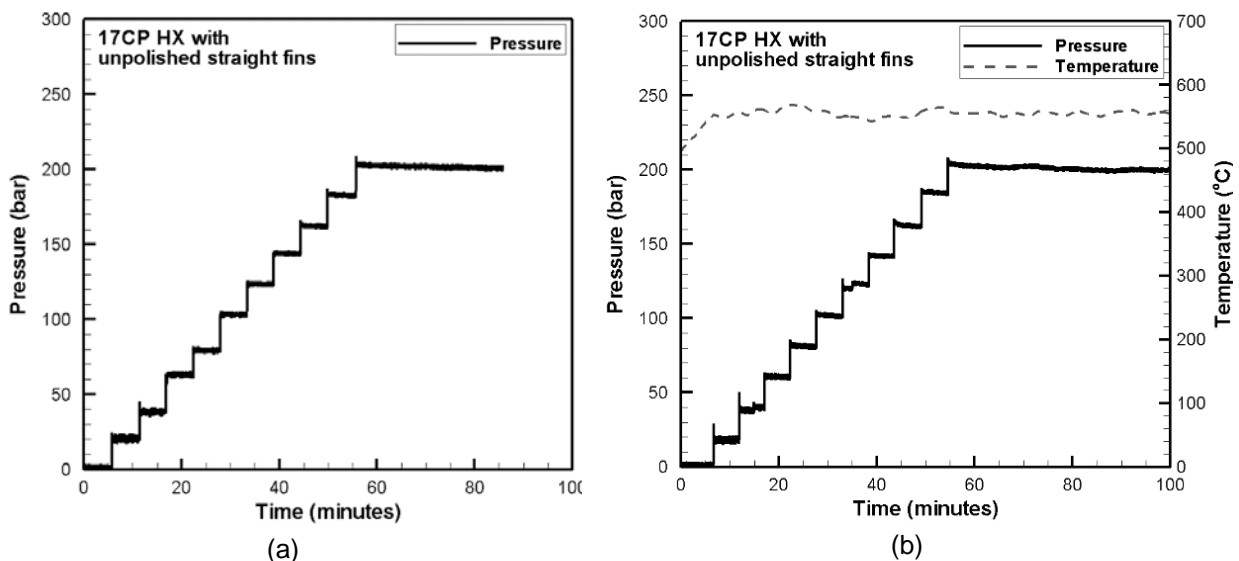


Figure 12. Results of static pressure tests on the 17-plate HX (a) static pressure test at ambient temperature, (b) static pressure test at operating temperature of 550 °C.

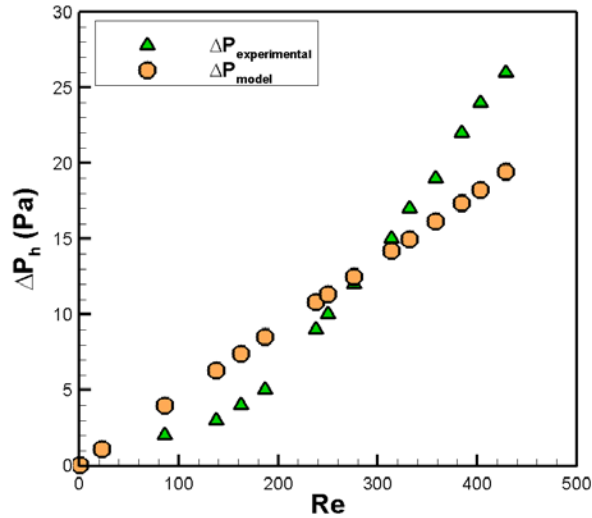


Figure 13. Comparison of pressure drop against Reynolds number between experiments and laminar flow theory. The bias error in the measurement was 7 Pa.

Figure 13 shows the results of pressure drop measurements of air under adiabatic condition. Also shown in Figure 13 is comparison of laminar flow theory pressure drop. The results indicate that in the range of tested flow rates (up to 208 SLPM corresponding to $Re=428$), the experimental pressure drop is relatively in agreement with prediction of laminar theory. It should be noted that the bias error in pressure drop measurement was 7 Pa; hence the error in the lower flow rates is considerable. However, the comparison is more favorable at Re greater than 200 but less than 400; the trends diverge in higher flow rates ($Re > 400$). A potential cause for the difference could be the large surface roughness of the PHX. Further post-processing treatments to improve surface finish are warranted.

Heat transfer experiments were performed by fixing hot air inlet temperature ($T_{h,i}$) to 200 °C. The required air flow rate was fixed at 140 SLPM (corresponding to 2.8 g/s). Based on sCO_2 pressure drop through the PHX, the CO_2 mass flow rate varied from the highest possible flow rate (~5 g/s) to about the mass flow rate as of air so the effectiveness of PHX was obtained for different heat capacity ratios ($C_r=C_{min}/C_{max}$). The variation of the PHX effectiveness and exchanged heat with C_r for $T_{h,i}$ of 200 °C test is depicted in Figure 14. The PHX effectiveness, ϵ , as seen in Figure 14 varies between 0.77-0.87 for C_r range of 0.11-0.75 where exchanged heat reached to about 350W for the lowest C_r (0.11) corresponding to NTU value about 1.9.

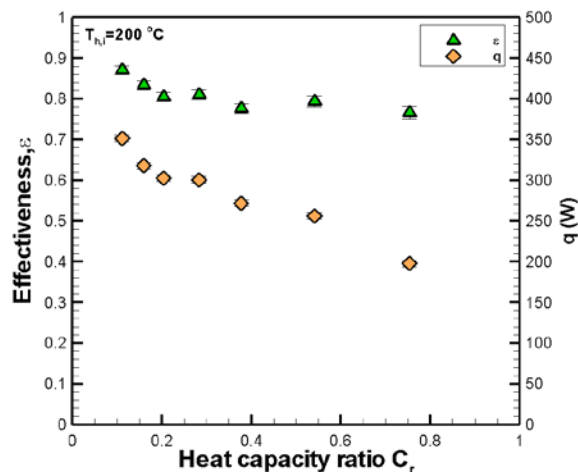


Figure 14. PHX effectiveness and exchanged heat variation with C_r

CONCLUSIONS

Design, fabrication, structural integrity verification and preliminary thermal-fluidic characterization of a novel AM PHX was presented in this paper. The design constraints included low pressure drop requirement on the hot (combustion) gas side and high internal pressure on the micro-pin plates. Additive manufacturing of the complex heat exchanger design was successfully completed and static pressure testing at design temperature was used to validate the structural integrity of the PHX. Pressure drop measurements showed good comparison at Re in excess of 200 but limited to 400 and for higher flow rates became higher than the laminar theory predictions. Heat transfer testing showed high effectiveness is possible with the PHX design; however, the testing was performed at temperatures lower than that of the sCO₂ cycle due to equipment and facility limitations.

REFERENCES

- [1] National Energy Technology Laboratory, Supercritical power cycles, <http://www.netl.doe.gov/research/coal/energy-systems/turbines/supercritical-co2-power-cycles>, accessed: April 2014.
- [2] Tuckerman, D. B., 1984, "Heat-Transfer Microstructures for Integrated Circuits," Ph.D. Thesis, Stanford University, Stanford, CA.
- [3] Peles, Y., Koşar, A., Mishra, C., Kuo, C. J., and Schneider, B., 2005, "Forced Convective Heat Transfer Across a Pin Fin Micro Heat Sink," *I. J. Heat Mass Transfer*, vol. 48, no. 17, pp. 3615-3627.
- [4] Azadian, S., We, L. Y., Niklasson, F., and Warren, R., 2001, "Precipitation in spray-formed in 718," *The minerals and materials society*, Vol. 6, pp. 617 – 626.
- [5] Thompson. J., 2014, "Relating microstructure to process variable in beam-based additive manufacturing of IN 718," Master's thesis, Wright State University, OH.
- [6] Rasouli, E., Naderi, C., Narayanan, V., 2017, "Pitch and Aspect Ratios Effects on Single-Phase Heat Transfer through Microscale Pin Fin Heat Sinks", *International Journal of Heat and Mass Transfer*, Vol. 118, pp. 416-428, <https://doi.org/10.1016/j.ijheatmasstransfer.2017.10.105>

ACKNOWLEDGEMENTS

Financial support for this work was provided by Office of Naval Research grant # N00014-16-1-2027 and Department of Energy grant # DE-FE0024064. The views and opinions of authors expressed herein do not necessarily state or reflect those of the United States Government or any agency thereof.

The authors acknowledge the assistance of Adam Strong and Andrew Shoats in fabrication of the heated channel and in cleaning the AM heat exchangers. Adam Strong also helped with characterization of the air-side pressure drop at ambient temperatures.